

Phonon transport across twin boundaries and twin superlattices

Kim López-Güell,¹ Nicolas Forrer,² Xavier Cartoixa,³ Ilaria Zardo,² and Riccardo Rurali¹

¹*Institut de Ciència de Materials de Barcelona, ICMAB-CSIC, Campus UAB, 08193 Bellaterra, Spain*

²*Departament Physik, Universität Basel, Klingelbergstrasse 82, 4056 Basel, Switzerland*

³*Departament d'Enginyeria Electrònica, Universitat Autònoma de Barcelona, 08193 Bellaterra, Barcelona, Spain*

(Dated: January 14, 2022)

Crystal phase engineering gives access to new types of superlattices where, rather than different materials, different crystal phases of the same material are juxtaposed. Here, by means of atomistic nonequilibrium molecular dynamics calculations, we study to what extent these periodic systems can be used to alter phonon transport, similarly to what has been predicted and observed in conventional superlattices based on heterointerfaces. We focus on twin superlattices in GaAs and InAs and highlight the existence of two different transport regimes: in one each interface behaves like an independent scatterer; in the other, a segment with a sufficiently large number of closely-spaced interfaces, is seen by propagating phonons as a metamaterial with its own thermal properties.

I. INTRODUCTION

The design of materials with tailor-made thermal properties is very attractive for several applications, ranging from efficient thermoelectrics [1, 2] to thermal management [3]. A way to engineer the phonon spectrum of a material, and thus to tune its thermal conductivity, is by creating superlattices, where wave interference creates forbidden energy bandgaps for phonons [4]. An additional interest in superlattices is that they allow, in principle, to observe the crossover from a particle- to a wave-like phonon transport regime, a topic of both fundamental and applied importance. When phonons travel across far apart interfaces, they are better described as particles that suffer multiple independent diffusive scattering events, each one characterized by the thermal boundary resistance of that interface [5, 6]. When the number of interfaces or their density increases, interference effects can build up and heat transport is better understood by taking into account the wave-nature of phonons. In the first situation the thermal conductance is tuned by controlling the number of interfaces; once the coherent regime kicks-in, on the other hand, the main control knob becomes the periodicity of the superlattice, which, in turn, determines the details of the phonon dispersion of the metamaterial, including the position and width of the phonon bandgap. This transition typically occurs by making the interface spacing of the same order of the phonon mean free path [7], a goal that can be achieved either increasing the interface density (i.e. reducing the superlattice period) or decreasing the temperature [8, 9]. Experimental indications of these effects have been reported in GaAs/AlAs [10] and perovskite oxides superlattices [11]. In this scenario, the quality of each individual interface is almost as important as their periodic arrangement [12]. Indeed, atomic-scale corrugations [13–16] and interfacial

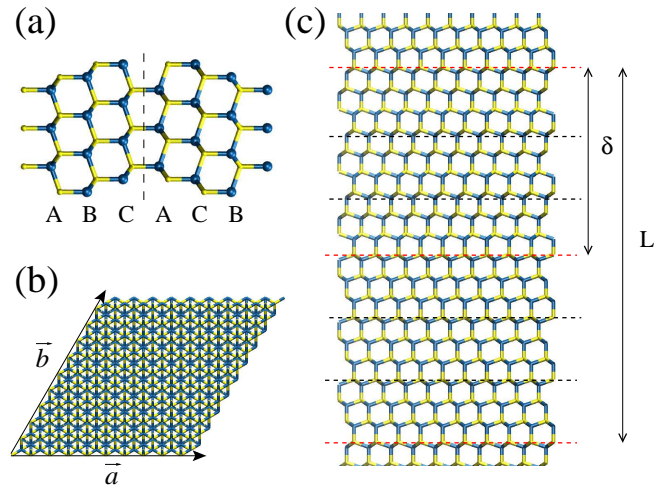


FIG. 1: (a) Zoomed view of a twin defect, showing the change from ABC to ACB stacking. (b) Cross-section view of the computational cell, where $a = b = 39.97$ Å for GaAs and 42.85 Å for InAs. (c) Segment of a TSL containing one full period, $L = 2\delta$, where δ is the separation between adjacent twins. The red dashed lines indicate the position of the twins, while the black dashed line show the unit cell of the zincblende, when the [111] crystal axis is taken to be parallel to the cartesian z-axis. Blue spheres represent Ga or In atoms and yellow spheres represent As atoms. .

chemical mixing [17, 18] have been shown to largely suppress the coherence of phonon transport. Therefore, the design of unconventional periodic structures, beyond the usual heterostructured superlattices, is attracting a considerable attention [19].

The increased control in the growth of semiconducting nanowires (NWs) [20, 21] has brought attention to a novel type of superlattice, where, rather than chemically different materials, different crystal phases of the same

material –typically zincblende and wurtzite segments of arsenides and phosphides– alternate with a well-defined periodicity. These crystal phase superlattices [22–24] are made of *homojunctions* that have (i) a minimal lattice mismatch and (ii) no chemical intermixing, and thus are virtually atomically flat. An even subtler kind of periodic superstructure that can be obtained in NWs is the so-called twin superlattice (TSL) [25, 26]. Here both the material and the crystal phase are the same throughout the entire NW length and the motif of the superlattice is determined by a periodic rotation of the crystal lattice, which induces the formation of a stacking planar defect that we refer to as twin boundary. TSLs of practical interest are made of zincblende materials that feature a 60° rotations of the crystal lattice, so that the ABC stacking along the [111] crystal axis switches to ACB after each twin boundary (see the sketch in Figure 1a); see Ref. 27 for other types of twin boundaries.

Twin boundaries are peculiar interfaces under many respects and defy the most common phenomenological approaches to the calculation of the thermal boundary resistance (TBR), i.e. the thermal resistance of an interface. The popular acoustic mismatch model (AMM) computes the TBR in terms of the mismatch of elastic properties of the constituent materials forming an interface. The rationale behind it is that a phonon impinging on the interface from one side is efficiently transmitted only if a suitable vibrational state, in terms of energy and momentum, exists on the other side. In a twin boundary, however, the materials on the two sides of the interface are identical and the AMM predicts no TBR, at odds with experimental results that have convincingly shown that they do have an effect on phonon dispersion [28] and with theoretical atomistic simulations of phonon transport [29, 30]. The diffuse mismatch model (DMM), on the other hand, returns the same finite value of the TBR that it would erroneously attribute to a homogeneous system with no interface [31]. Previous theoretical calculations, combining molecular dynamics and Green’s functions, showed that the TBR of twin boundaries in GaP and InP is determined by the rotation of the phonon polarization vectors and by local structural distortion at the interface [30]. This explains why simplified models based on the mismatch of the elastic properties cannot capture phonon scattering at twin boundaries and call for modeling approaches that explicitly account for the atomic structure of the interface.

II. COMPUTATIONAL METHODS

We perform non-equilibrium molecular dynamics (NEMD) simulations with the LAMMPS code [32] and a

Tersoff-type interatomic potential [33] parameterized by Nordlund and coworkers [34]. We consider GaAs and InAs computational cells with the transport direction parallel to the cubic [111] crystal axis, which we take to be the z coordinate direction. This choice is dictated by the fact that this is growth direction of nanowires along which twin boundaries can be formed during growth. The ends of the computational cells are connected to Nose-Hoover thermostats at temperatures T_H and T_C , while the rest of the system evolves according to the micro-canonical ensemble. We start from the 6-atom unit cell of zincblende crystals, which has the [111] crystallographic direction parallel to the z -axis and construct $10 \times 10 \times M$ supercells. We take $M = 90$ for the study of isolated interfaces and $M = 180$ for systems featuring multiple interfaces, i.e. a superlattice segment. We apply periodic boundary conditions along x - and y -axis. The TBR is calculated as $\Delta T/J$, where ΔT is the temperature jump at the interface and J is the heat flux [5] (see Refs. [6, 35] for a more general discussion).

After the simulation starts, a thermal gradient rapidly builds up, but we nevertheless disregard the first $3 \cdot 10^6$ steps to allow a proper equilibration of the system. In all cases this time interval proved to be sufficient to reach the nonequilibrium steady-state. Indeed, after this equilibration interval, not only the time evolution of the local temperature along z is roughly constant, but also the rate of energy injected and extracted by the hot and cold thermostats are the same, within numerical fluctuations. After the steady-state is reached, we average the heat flux and the temperature over runs that go from 7.5 to $30 \cdot 10^6$ steps. We apply a temperature difference $T_H - T_C$ equal to 100 K, varying T_C and T_H in order to obtain a different average temperature, T_M . Notice that below the Debye temperature the use of classical dynamics, where quantum effects are neglected, should be handled with care. Yet, attempts at correcting for quantum features in low temperature molecular dynamics provided inconclusive and contrasting results [36]. We address the effect of this limitation in detail below.

NEMD notoriously suffers from finite-size effects and the usual procedure to estimate the thermal conductivity of a material requires running simulations in increasingly large cells. In this work, however, our goal is either computing TBRs, which is much less sensitive to cell sizes [37], or studying the dependence of the thermal resistance in multi-interface systems, where we compare results obtained in cells of the same size.

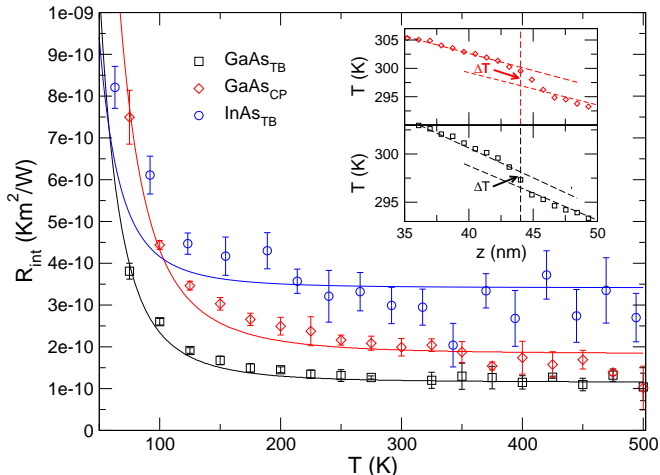


FIG. 2: TBR as function of temperature of a single twin boundary in GaAs and InAs and of a crystal phase interface in GaAs. The continuous lines are fits of the computed data to a T^{-3} dependence of the TBR. The inset shows the temperature profile, $T(z)$ around a crystal phase interface (top) and a twin boundary in GaAs (bottom). The temperature jump, ΔT , that is the signature of the TBR and that is used to compute it, is indicated.

III. RESULTS AND DISCUSSION

A. Isolated twin boundary

As a first step of our study we have calculated the TBR as a function of the interface temperature of a twin boundary in GaAs and InAs, as displayed in Figure 2. To this end, after reaching the nonequilibrium steady-state, we estimate the heat flux from the energy per unit time injected/extracted by the hot/cold thermostats and the thermal gradient from the averaged temperature profile, $T(z)$; representative examples are provided in the insets. The results obtained are similar to previous reports of GaP and InP, showing that the physical effects are general and do not qualitatively depend on the material or on the classical potential used to describe interatomic interactions (Vashista potential for phosphides [38, 39], Nordlund for arsenides [34]). In the case of GaAs, we add for comparison a crystal phase interface between segments of zincblende and wurtzite crystals (red diamonds in Figure 2), which is also a class of important interfaces in NW physics [23, 24]. In agreement with the results obtained with GaP and InP, we find a TBR of the order of $2 \times 10^{-10} \text{ K m}^2 \text{ W}^{-1}$, smaller than conventional heterointerfaces, but slightly larger than the one obtained for the corresponding twin boundary (black squares in Figure 2). The continuous lines are fits of the calculated

data to T^{-3} , the temperature dependence predicted by the same phenomenological models that fail to account for the TBR [5] of twin boundaries. While this temperature dependence seems to be reasonable for both the twin boundary and the crystal phase interface in GaAs, in the case of InAs we obtain a somewhat more abrupt saturation to the high temperature value, preventing a satisfactory fit to a T^{-3} decay, particularly at low temperatures. A possible reason is the fact that the Debye temperature of InAs is 80 K lower than that of GaAs and thus low temperature results obtained within classical molecular dynamics are comparatively less accurate in the former case.

B. Increasing the number of twins

Now that we have established that individual twin boundaries in arsenides behave similarly to conventional heterointerfaces, though with a smaller associated TBR, we move to the study of multiple interfaces. Our goal is assessing to what extent TSLs, periodic superstructures made of an ordered sequence of twins, behave like conventional superlattices in altering phonon transport. In a first set of computational experiments, we have considered an increasing number of twin boundaries, $1 \leq N \leq 20$, located in the central part of the computational cell. The separation between neighboring twins, δ , is fixed, so that the twinned region has a thickness equal to $N\delta$. We take $\delta = 29.4 \text{ \AA}$ for GaAs and 31.5 \AA for InAs, i.e. three unit cells along the [111] crystal axis. Notice that the size of the computational cell along the transport direction has been doubled with respect to the one used for the results of Figure 2. In this way we guarantee that the twinned region is sufficiently separated from the thermostats, also for the largest values of N .

We computed $\Delta R = R_N - R_0$, where R_N and R_0 are the thermal resistances of a system with N and zero twin boundaries. The thermal resistances are computed as $I/\Delta T$, where I is the heat current and ΔT is evaluated between the values of the z coordinate axis z_i and z_f , taken to be sufficiently far from the thermal reservoirs to avoid the usual non linearities of the temperature. We considered two different values of the average temperature $T_M = (T_H + T_C)/2$: a low temperature case, with $T_M = 100 \text{ K}$ and a higher temperature $T_M = 300$ and 250 K , for GaAs and InAs, respectively, which is of the order of the Debye temperature of each material ($T_D = 360 \text{ K}$ for GaAs and $T_D = 280 \text{ K}$ for InAs).

The results for GaAs and InAs at $T_M = 100 \text{ K}$ are shown in Figure 3. If each twin boundary acted as an independent scatterer for phonons, ΔR should increase linearly and its slope would be related to the TBR of an

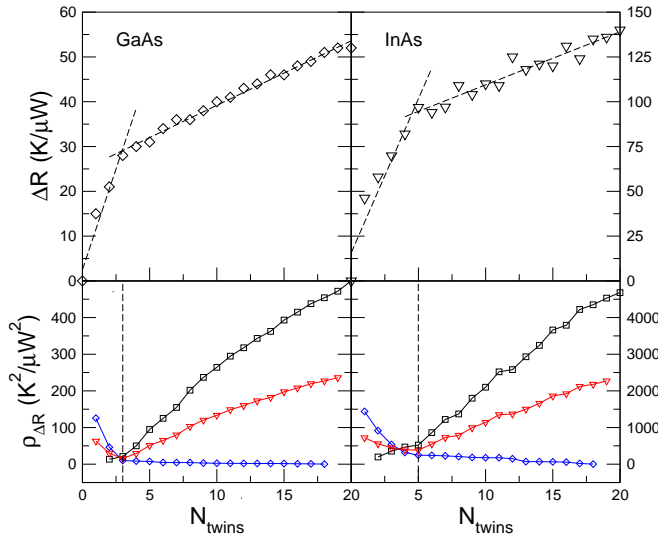


FIG. 3: (Top) Thermal resistance as a function of the number of twins in GaAs and InAs, at low temperature. ΔR is defined as $R_N - R_0$, where R_N and R_0 are the thermal resistances of a system with N and zero twin boundaries. (Bottom) Mean of the residual squares of two linear fits of $\Delta R[0, N]$ and $\Delta R[N, 20]$ as a function of N (red triangles); the individual residual squares of each fit is also shown (black squares and blue diamonds). The mean has a minimum at $N = 3$ and $N = 5$ for GaAs and InAs, respectively. The corresponding linear fits are shown in the upper panels with a dashed line.

individual twin. Indeed, this is what we observe at the beginning for the low temperature simulations of both materials (see Figure 3). However, as the number of twins increases the behavior changes and a different transport regime can be identified. Once more than 3-5 twins are stacked next to each other, a collective effect builds up and the slope of ΔR changes. Notice that a hint of the coherent behaviour that develops in the many-twin limit was already present in the low-twin transport regime. Indeed, as better seen in the low temperature results of Figure 3, the value of ΔR for two twins is less than twice the value it takes of the individual twin, an indication of the interaction between neighbouring twins for the chosen value of δ . In order to establish in a quantitative way for which value of N the slope changes, we have carried out two linear fits of the computed ΔR in the intervals $[0, N]$ and $[N, 20]$, varying N , and plotted the mean residual of squares. We found that the best fits are obtained for $N = 3$ and $N = 5$ for GaAs and InAs, respectively. We also checked if the fit can be improved significantly by assuming more than two linear regressions, but this was not the case.

In the higher temperature case, where $T_M = 250$ or

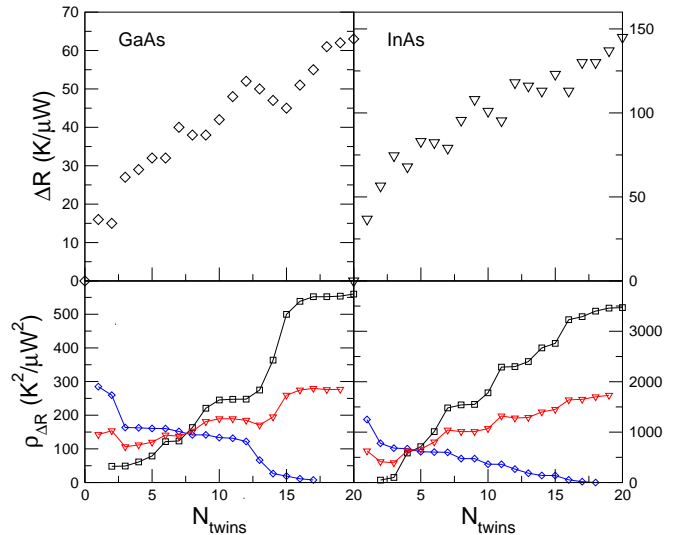


FIG. 4: (Top) Thermal resistance as a function of the number of twins in GaAs and InAs, at room temperature. ΔR is defined as $R_N - R_0$, where R_N and R_0 are the thermal resistances of a system with N and zero twin boundaries. (Bottom) Mean of the residual squares of two linear fits of $\Delta R[0, N]$ and $\Delta R[N, 20]$ as a function of N (red triangles); the individual residual squares of each fit is also shown (black squares and blue diamonds). No clear minima emerge.

300 K, such a distinction between two transport regimes is more difficult to make. While by visual inspection it seems that for both materials the slope changes at $N \sim 3$, no clear minima of the mean of the residual squares emerge (see Figure 4).

We recall here that at low temperatures, the results obtained from classical molecular dynamics cannot be taken quantitatively. Assuming that atoms move according to Newton's laws implies that phonon population follows Maxwell-Boltzmann, rather than Bose-Einstein statistics and this is a good approximation only at sufficiently high temperatures. Simplified schemes to correct for these effects include a temperature renormalization [40–43] (the results obtained at a nominal temperature T_{MD} are actually valid at a different temperature, T_Q) or using quantum, rather than classical specific heat, when it is required for the calculation of the thermal conductivity [44, 45]. However, even within the more general discussion of Berens *et al.* [46], the result of properly accounting for quantum effects is a temperature dependent correction of the thermodynamical variables calculated that can, for instance, be responsible for the low temperature behavior of the individual InAs twin boundary discussed above. The results of Figure 3, however, have all been obtained at the same temperature and thus any

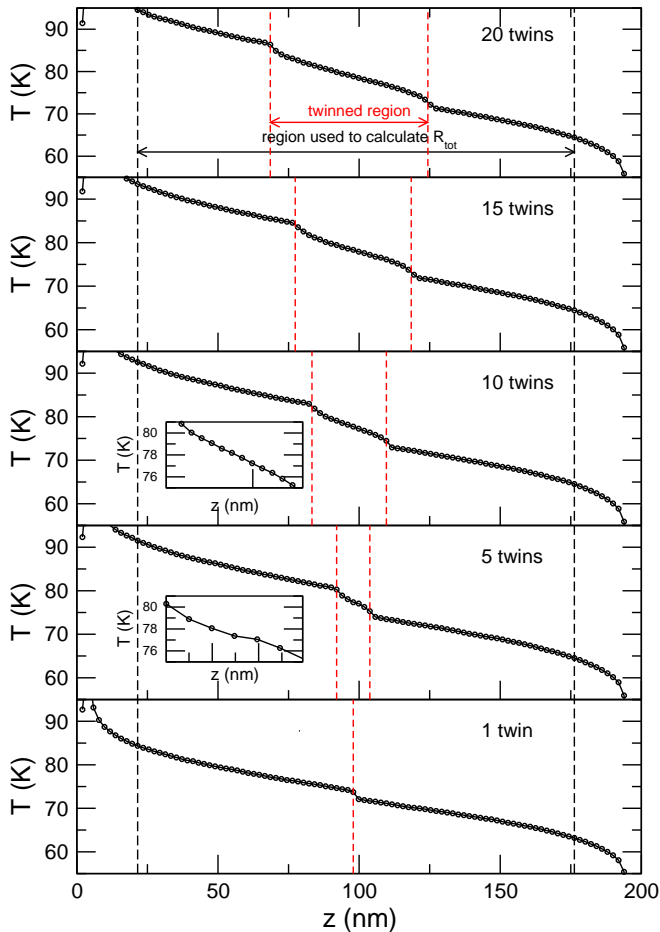


FIG. 5: Temperature profile, $T(z)$ for a GaAs system with $N = 1, 5, 10, 15,$ and 20 twins with a constant intertwin separation, δ and with $T_M = 100$ K. The red dashed lines indicate the position of the first and last twin boundary (i.e., the thickness of the twinned region). The coordinates z_i and z_f , used to evaluate ΔT to yield ΔR in Figure 3 are marked by the red dashed lines. Inset display a zoomed view of $T(z)$ of the twinned region.

small correction to the computed values would affect in a similar way all data points. Clearly, we are not concerned here with the specific values of ΔR , but rather on highlighting two different transport regimes. In this sense, our results are reliable and provide a valuable insight of the underlying physics.

C. Temperature profiles

The spatial dependence of the temperature along the transport direction is essential in NEMD not only to esti-

mate the TBR, but also to compute the thermal conductivity of a homogeneous system. Indeed, even when the temperature of the reservoirs is fixed, it is safer to rely on the thermal gradient of a central region of the simulation cell, rather than on the nominal thermal bias, $T_H - T_C$. Additionally, $T(z)$ conveys an important physical insight in presence of interfaces. In Figure 5 we plot $T(z)$ for a GaAs system with 1, 5, 10, 15, and 20 twin boundaries at $T_M = 100$ K. The case with one single twin resembles the temperature profile shown in the inset of Figure 2, although here results have been obtained in a larger computational cell. The temperature discontinuity is small, but clearly observable and it occurs exactly where the twin boundary is located. Next, we consider the case of five twin boundaries. Although it is not possible to observe the signature of the five interfaces, it is clear that within the twinned region $T(z)$ still exhibits a certain structure (see the zoomed view in the inset). In the rest of the cases displayed here ($N > 5$), on the other hand, the twinned region behaves at all effects as a *metamaterial* with its own thermal resistance. Phonons experience a TBR between pure GaAs segments and a central TSL segment. Remarkably, the TBR to enter/exit the TSL region are, though small, clearly visible and similar in all the cases. Conversely, within the twinned region $T(z)$ is linear, as expected in a homogeneous material (see the inset for $N = 10$). See the Supporting Information for the results of GaAs at $T_M = 300$ K and for InAs at $T_M = 100$ and 250 K.

The analysis of Figure 5 helps rationalize the dependence of ΔR presented above. Once the twinned region is seen by the propagating phonons as a segment of TSL with its own resistivity, ρ_{TSL} , the total resistance is simply

$$R = \frac{1}{A} \int_{z_i}^{z_i^t} \rho_{GaAs}[T(z)]dz + \frac{1}{A} \int_{z_i^t}^{z_f^t} \rho_{TSL}[T(z)]dz + \frac{1}{A} \int_{z_f^t}^{z_f} \rho_{GaAs}[T(z)]dz \quad (1)$$

where $L_z = z_f - z_i$ is the total length probed, A is the cross-section, ρ_{GaAs} is the temperature dependent thermal resistivity of GaAs; the initial and final coordinates of the TSL segment are $z_i^t = L_z/2 - N\delta/2$ and $z_f^t = L_z/2 + N\delta/2$. If, for simplicity, we drop the temperature dependence of ρ_{TSL} and ρ_{GaAs} , the resistance simply reads $R = N\delta\rho_{TSL}/A + (L_z - N\delta)\rho_{GaAs}/A$. Therefore, if we look back at Figure 3, we can distinguish two transport regimes: at first ΔR increases because the number of twin interfaces increases; next it increases because the length of the more resistive TSL segment increases. In the first case phonons see the twin boundaries as individual scatterers and the increase of ΔR is dictated by the TBR of each twin; in the second case the twinned region is seen as a TSL with its own conductivity, which

depends on the superlattice design parameters, e.g. t period.

These considerations suggest that a different balance between the TBR of the individual interface and the resistivity of the ideal superlattice, i.e. with a very large N , could result in a different dependence of ΔR on t number of twins. In particular, if the TSL was considerably less resistive than the pure untwinned systems, a different collective interface behavior shows up should first increase to a maximum and then decrease.

D. Increasing the density of twins

Finally, we report the results obtained in a different kind of computational experiments, in order to further corroborate our conclusions. Now, rather than varying the number of twins and fixing their separation, we consider the opposite: we consider a fixed number of six twin boundaries and vary gradually the separation between neighboring interfaces. If the transport regime was fully incoherent and each interface scattered phonons independently from the others, the total thermal resistance should be constant, as all the systems contain the same number of twin boundaries. Our results for GaAs are displayed in Figure 6 and capture a rather different situation. While for large separations ($\delta > 60$ nm) the additional resistance introduced by the twin boundaries is almost constant, when they are brought together it decreases, a clear indication that ΔR does not simply result from the sum of independent scattering events. It is interesting that here the trend is quite clear also for room temperature case, while such an observation was not fully conclusive when we varied the number of twin defects (see Figure 4).

IV. CONCLUSIONS

In summary, we have carried out computational experiments based on nonequilibrium molecular dynamics and provided clear fingerprints of the fact that twin superlattices behave similarly to their conventional counterparts, where segments of different materials repeat periodically. Namely we have shown that (i) isolated twin defects have a small, but finite thermal boundary resistance; (ii) when a sufficiently high number of twin defects are stacked close to each other, phonons see the twinned region as an homogeneous (meta)material; (iii) the way

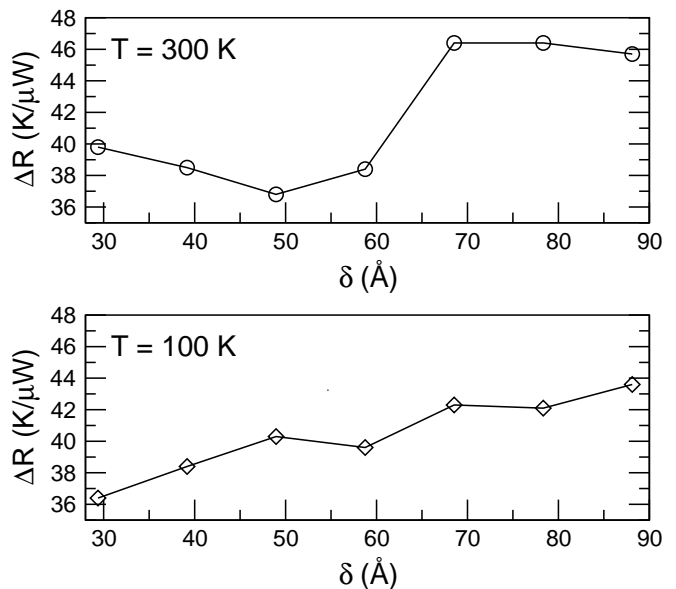


FIG. 6: Thermal resistance as a function of the intertwin separation, δ , for a GaAs system with 6 twin boundaries and for (top) $T_M = 300$ K and (bottom) 100 K.

engineering can become an effective way to design materials with desired phononic properties and to manipulate phonons similar to conventional superlattices, but with additional advantages, such as defect-free and atomically abrupt interfaces.

Acknowledgments

KLG and RR acknowledge financial support by the Agencia Estatal de Investigación under grant FEDER-MAT2017-90024-P, and the Severo Ochoa Centres of Excellence Program under grant CEX2019-000917-S, and by the Generalitat de Catalunya under grant no. 2017 SGR 1506. IZ acknowledges financial support by the European Research Council (756365) and the Swiss National Science Foundation research grant (project grant no. 184942). We thank the Centro de Supercomputación de Galicia (CESGA) for the use of their computational resources.

[1] M. Zebarjadi, K. Esfarjani, M. S. Dresselhaus, Z. F. Ren, and G. Chen, *Energy Environ. Sci.* **5**, 5147 (2012).

[2] G. Benenti, G. Casati, K. Saito, and R. S. Whitney,

- Physics Reports **694**, 1 (2017).
- [3] A. L. Moore and L. Shi, *Materials Today* **17**, 163 (2014).
- [4] M. Maldovan, *Nat. Mater.* **14**, 667 (2015).
- [5] E. T. Swartz and R. O. Pohl, *Rev. Mod. Phys.* **61**, 605 (1989).
- [6] R. Rurali, L. Colombo, X. Cartoixà, O. Wilhelmsen, T. T. Trinh, D. Bedeaux, and S. Kjelstrup, *Phys. Chem. Chem. Phys.* **18**, 13741 (2016).
- [7] M. V. Simkin and G. D. Mahan, *Phys. Rev. Lett.* **84**, 927 (2000).
- [8] B. Yang and G. Chen, *Phys. Rev. B* **67**, 195311 (2003).
- [9] J. Garg and G. Chen, *Phys. Rev. B* **87**, 140302 (2013).
- [10] M. N. Luckyanova, J. Garg, K. Esfarjani, A. Jandl, M. T. Bulsara, A. J. Schmidt, A. J. Minnich, S. Chen, M. S. Dresselhaus, Z. Ren, et al., *Science* **338**, 936 (2012).
- [11] J. Ravichandran, A. K. Yadav, R. Cheaito, P. B. Rossen, A. Soukiassian, S. J. Suresha, J. C. Duda, B. M. Foley, C.-H. Lee, Y. Zhu, et al., *Nat. Mater.* **13**, 168 (2013).
- [12] Y. K. Koh, Y. Cao, D. G. Cahill, and D. Jena, *Adv. Funct. Mater.* **19**, 610 (2009).
- [13] T. Ruf, J. Spitzer, V. F. Sapega, V. I. Belitsky, M. Cardona, and K. Ploog, *Phys. Rev. B* **50**, 1792 (1994).
- [14] Y.-C. Wen, C.-L. Hsieh, K.-H. Lin, H.-P. Chen, S.-C. Chin, C.-L. Hsiao, Y.-T. Lin, C.-S. Chang, Y.-C. Chang, L.-W. Tu, et al., *Phys. Rev. Lett.* **103**, 264301 (2009).
- [15] Z. Tian, K. Esfarjani, and G. Chen, *Phys. Rev. B* **89**, 235307 (2014).
- [16] S. Mei and I. Knezevic, *J. Appl. Phys.* **118**, 175101 (2015).
- [17] E. S. Landry and A. J. H. McGaughey, *Phys. Rev. B* **79**, 075316 (2009).
- [18] S. C. Huberman, J. M. Larkin, A. J. H. McGaughey, and C. H. Amon, *Phys. Rev. B* **88**, 155311 (2013).
- [19] R. Frieling, M. Radek, S. Eon, H. Bracht, and D. E. Wolf, *Appl. Phys. Lett.* **105**, 132104 (2014).
- [20] N. Wang, Y. Cai, and R. Zhang, *Mater. Sci. Eng. R* **60**, 1 (2008).
- [21] P. Caroff, J. Bolinsson, and J. Johansson, *IEEE Journal of Selected Topics in Quantum Electronics* **17**, 829 (2011).
- [22] Q. Xiong, J. Wang, and P. C. Eklund, *Nano Lett.* **6**, 2736 (2006).
- [23] P. Caroff, K. A. Dick, J. Johansson, M. E. Messing, K. Deppert, and L. Samuelson, *Nat. Nanotech.* **4**, 50 (2009).
- [24] K. A. Dick, C. Thelander, L. Samuelson, and P. Caroff, *Nano Lett.* **10**, 3494 (2010).
- [25] R. E. Algra, M. A. Verheijen, M. T. Borgström, L.-F. Feiner, G. Immink, W. J. P. van Enkevort, E. Vlieg, and E. P. A. M. Bakkers, *Nature* **456**, 369 (2008).
- [26] T. Burgess, S. Breuer, P. Caroff, J. Wong-Leung, Q. Gao, H. Hoe Tan, and C. Jagadish, *ACS Nano* **7**, 8105 (2013).
- [27] E. L. Wood and F. Sansoz, *Nanoscale* **4**, 5268 (2012).
- [28] M. De Luca, C. Fasolato, M. A. Verheijen, Y. Ren, M. Y. Swinkels, S. Kölling, E. P. A. M. Bakkers, R. Rurali, X. Cartoixà, and I. Zardo, *Nano Lett.* **19**, 4702 (2019).
- [29] A. Porter, C. Tran, and F. Sansoz, *Phys. Rev. B* **93**, 195431 (2016).
- [30] J. Carrete, M. López-Suárez, M. Raya-Moreno, A. S. Bochkarev, M. Royo, G. K. H. Madsen, X. Cartoixà, N. Mingo, and R. Rurali, *Nanoscale* **11**, 16007 (2019).
- [31] This is a known shortcoming of the DMM. If one considers a homogeneous system, without any physical interface, and applies the recipe of the DMM across a fictitious boundary, a finite TBR is obtained.
- [32] S. Plimpton, *J. Comput. Phys.* **117**, 1 (1995), URL <http://lammps.sandia.gov/>.
- [33] J. Tersoff, *Phys. Rev. B* **39**, 5566 (1989).
- [34] K. Nordlund, J. Nord, J. Frant, and J. Keinonen, *Comp. Mater. Sci.* **18**, 283 (2000).
- [35] R. Dettori, C. Melis, X. Cartoixà, R. Rurali, and L. Colombo, *Adv. Phys. X* **1**, 246 (2016).
- [36] O. N. Bedoya-Martínez, J.-L. Barrat, and D. Rodney, *Phys. Rev. B* **89**, 014303 (2014).
- [37] R. Rurali, X. Cartoixà, and L. Colombo, *Phys. Rev. B* **90**, 041408 (2014).
- [38] C. I. Ribeiro-Silva, J. P. Rino, L. G. V. Gonçalves, and A. Picinin, *J. Phys.: Condens. Matter* **23**, 055801 (2011).
- [39] P. S. Branicio, J. P. Rino, C. K. Gan, and H. Tsuzuki, *J. Phys.: Condens. Matter* **21**, 095002 (2009).
- [40] J. Hu, X. Ruan, and Y. P. Chen, *Nano Lett.* **9**, 2730 (2009).
- [41] J. Hu, X. Ruan, Z. Jiang, and Y. P. Chen, *AIP Conf. Proc.* **1173**, 135 (2009).
- [42] M. Saiz-Bretín, A. Malyshev, F. Domínguez-Adame, D. Quigley, and R. Römer, *Carbon* **127**, 64 (2018).
- [43] A. Soleimani, H. Araghi, Z. Zabihi, and A. Alibakhshi, *Comp. Mater. Sci.* **142**, 346 (2018).
- [44] C. Melis, R. Dettori, S. Vandermeulen, and L. Colombo, *Eur. Phys. J. B* **87**, 96 (2014).
- [45] C. Melis and L. Colombo, *Phys. Rev. Lett.* **112**, 065901 (2014).
- [46] P. H. Berens, D. H. J. Mackay, G. M. White, and K. R. Wilson, *J. Chem. Phys.* **79**, 2375 (1983).